Available online at www.sciencedirect.com

ScienceDirect

Procedia Structural Integrity 79 (2026) 433–439

Structural Integrity
Procedia

www.elsevier.com/locate/procedia

28th International Conference on Fracture and Structural Integrity - 3rd Mediterranean Conference on Fracture and Structural Integrity

Fatigue crack growth behavior of a high entropy alloy

Costanzo Bellini[a], Vittorio Di Cocco[a], Francesco Iacoviello[a], Filippo Berto[b], Stefano Natali[b], Cristian Vendittozzi[b,*]

[a]*DICeM - University of Cassino and Southern Lazio, Via G. Di Biasio 43, Cassino, FR 03043, Italy*
[b]*Department of Chemical Engineering Materials Environment, Sapienza University of Rome, Via Eudossiana 18, 00184 Roma, Italy*

Abstract

Compact-tension (CT) specimens of the equiatomic Co–Cr–Fe–Mn–Ni high-entropy (Cantor) alloy were cycled to failure and the fracture surfaces examined by scanning electron microscopy. The surface separates into a fatigue-propagation region and a final overload zone. The fatigue region is predominantly transgranular and exhibits a tortuous, step-rich morphology with short secondary cracks—features consistent with heterogeneous slip in a low-stacking-fault-energy FCC alloy and with roughness-induced deflection. Localized parallel markings compatible with striation-like features appear in select high-magnification areas, although continuous periodic striations are not uniformly resolved. Final fracture proceeds by ductile microvoid coalescence, producing a dimpled morphology with occasional particle imprints at dimple bases. No pervasive intergranular decohesion is observed. Taken together, these observations indicate that fatigue-crack advance reflects a synergy of intrinsic crack-tip plasticity and extrinsic shielding that promotes crack-path tortuosity. Crack-closure was not quantified; interpretations are strictly fractography-based.

Peer-review under responsibility of IGF28 - MedFract3 organizers

Keywords: high-entropy alloy; Cantor alloy; fatigue-crack growth; ΔK_{th}; Paris law; fractography; transgranular fracture; microvoid coalescence.

* Corresponding author. Tel.: +39 0644585-646
E-mail address: cristian.vendittozzi@uniroma1.it

Peer-review under responsibility of IGF28 - MedFract3 organizers
10.1016/j.prostr.2025.12.354

1. Introduction

High-entropy alloys (HEAs) with face-centered cubic (FCC) structures have garnered sustained interest because several compositions combine high strength with outstanding damage tolerance, particularly at low temperatures. Among them, the equiatomic Co–Cr–Fe–Mn–Ni "Cantor alloy" has become the canonical reference system owing to its single-phase FCC solid solution, low stacking-fault energy (SFE), and unusual synergy of deformation mechanisms (partial dislocation activity, profuse stacking faults, and deformation twinning) that sustain work hardening and delay localization. Pioneering studies demonstrated that this alloy exhibits exceptional fracture resistance and ductility at cryogenic temperatures, establishing a compelling motivation to interrogate its resistance to cyclic crack advance, Gludovatz B. et al. (2014, 2016 and 2022). Building on this damage-tolerance foundation, systematic FCG measurements on the Cantor alloy revealed a strong sensitivity of near-threshold and Paris-law behavior to temperature and load ratio, R. In an influential study, Keli V.S. et al. (2017) quantified crack-growth rates from near-threshold into the Paris regime between cryogenic and ambient temperatures, showing that the alloy's threshold ΔK_{th} generally increases with decreasing temperature and that crack growth is retarded at low temperatures relative to room temperature. Mechanistically, this trend was linked to enhanced roughness-induced crack closure and twinning-assisted crack-tip shielding as the alloy's twinning propensity rises with decreasing SFE at cryogenic conditions [4]. A subsequent, extended mapping across temperatures and R-ratios reinforced these conclusions and provided widely cited Paris-law parameters for design comparisons, Keli V.S. et al. (2019). Together, these works anchor the view that the Cantor alloy's FCG resistance derives not only from intrinsic crack-tip plasticity but also from extrinsic shielding mechanisms that are promoted as temperature declines. Classical load-history effects also appear operative in this HEA, with important Cantor-specific nuances. In particular, tensile overloads—common in variable-amplitude spectra—produce marked retardation of subsequent growth rates. Has been demonstrated that overload-induced deformation twinning in the plastic wake contributes to roughness and residual crack-wake shielding, thereby extending retardation relative to baseline constant-amplitude growth. Follow-on work showed that overloads can also induce crystallographic texture that further modulates the post-overload crack path and shielding, underscoring the coupling between local microstructure and FCG resistance in this alloy family, Tu-Ngoc Lam et al. (2020 and 2023). These observations align with broader fatigue literature on overload effects while emphasizing the role of twinning in a low-SFE HEA as a distinctive wake-hardening and roughness lever, Tu-Ngoc Lam et al. (2020). Microstructural state is another axis that strongly impacts FCG in the Cantor alloy. Recent studies highlight that grain refinement and topology (e.g., harmonic or gradient microstructures) can shift near-threshold behavior and Paris-law slopes by altering the balance between slip/twin activity, crack-path tortuosity, and closure. At the extreme, nanocrystalline variants demonstrate modified short-crack kinetics and distinct fractography relative to coarse-grained states, emphasizing the need to consider scale effects when comparing datasets, Linhu Shi et al. (2023) and Pillmeier S. et al. (2024). More broadly, datasets aggregating HEA fatigue results point to microstructure-induced scatter near ΔKth and in the low-ΔK Paris regime, where small changes in SFE, short-range order, or residual stresses can disproportionately affect crack-tip shielding and effective driving force, Chen S. et al. (2022). Alloying additions provide a complementary route to shift the Cantor alloy' s deformation landscape. Minor W additions (~2 - 3 at.%) preserve the FCC matrix in the as-cast state, increase the atomic size mismatch δ and the valence electron concentration (VEC, an empirical FCC/BCC stability indicator), and—after heat treatment—promote Fe_7W_6 grain-boundary precipitation; in parallel, strength and hardness increase while ductility decreases across processing routes, Brotzu A. et al. (2022). These trends underscore how composition and thermomechanical history co-determine the crack-tip micromechanics that govern near-threshold and Paris-regime behavior. A useful comparative lens is provided by medium-entropy FCC alloys such as CrCoNi, which share many deformation characteristics with the Cantor system. At cryogenic temperatures, CrCoNi variants exhibit similarly exceptional toughness and low SFE-enabled twinning, and several reports document slowed FCG and elevated thresholds compared with room temperature. These comparisons suggest that metastability-assisted mechanisms (TWIP/TRIP) are a unifying design lever for FCG resistance across low-SFE FCC multi-principal alloys, while also highlighting composition-specific differences in twinning kinetics and crack-tip process-zone micromechanics, Gludovatz B. et al. (2016). Despite this progress, key questions remain. First, the quantitative coupling among SFE, twinning propensity, and effective crack-tip shielding in the Cantor alloy is not fully resolved across microstructural states; this limits transferability of Paris-law constants between processing routes or product forms. Second, the transition from small- to long-crack behavior—where microstructural barriers, crack-path tortuosity, and closure evolve rapidly—deserves further attention, particularly near threshold where data scatter is largest. Third, while overload-induced retardation and texture effects are clearly present, predictive models that incorporate twin-mediated wake hardening and roughness in a mechanistic fashion are still emerging. Finally, environment- and frequency-dependent effects remain relatively underexplored compared with temperature and R-ratio, yet are essential for service-relevant life predictions. Addressing these gaps in the specific context of the Cantor alloy can refine our understanding of how metastable plasticity at the crack tip governs growth kinetics across regimes, and it can inform microstructure-aware design strategies for HEAs in fatigue-critical applications, Gludovatz, B. et al. (2022); Keli V.S. et al. (2017 and 2019) ; Tu-Ngoc Lam et al. (2020 and 2023).

Nomenclature

A	radius of
B	position of
C	further nomenclature continues down the page inside the text box

2. Materials and Methods

2.1. Alloy preparation and composition

An equiatomic Co – Cr – Fe – Mn – Ni high-entropy (Cantor) alloy was produced by melting the alloying elements (⩾99.9% purity Co, Cr, Fe, Mn, Ni) in a centrifugal casting melting furnace (spin-casting configuration). The charge was melted under an inert Ar atmosphere and spin-cast into a preheated ceramic mold; the centrifugal action promoted rapid, defect-free filling and solidification. To enhance chemical homogeneity, the charge was re-melted and spin-cast multiple times (3–5 cycles) with flipping between cycles. Chemical composition was verified by SEM/EDS on polished sections and confirmed near-equiatomic levels for Co, Cr, Fe, Mn, and Ni. X-ray diffraction (Cu Kα) on the as-tested material indicated a single-phase FCC structure. Unless stated otherwise, specimens were tested in the as-cast condition.

2.2. Specimen geometry and machining

Compact-tension (CT) specimens were machined from plate with nominal dimensions W = 50 mm and B = 10 mm (net thickness), following ASTM E647 for fatigue-crack growth testing. The initial machined notch length was $a_0/W = 0.50$. Side grooves were not introduced unless specified; when used, each groove had depth ~0.1B with root radius ~0.25 mm to promote through-thickness crack straightness. The notch face and crack-plane surfaces were ground and polished to at least a P1200 finish parallel to the crack-growth direction.

Specimens were cycled to failure to capture the final fracture surface.

2.3. Post-fracture examination (SEM/EDS)

After failure, fracture surfaces were rinsed in acetone and ultrasonicated for 10 min to remove loose debris. Scanning electron microscopy (SEM) was performed at an accelerating voltage of 15 kV and working distance of ~15 mm. For each specimen, the crack origin was located via beach/arrest marks at low magnification, then imaged at progressively higher magnifications. Global overviews (low magnification) located the fatigue-propagation region, the transition, and the final overload zone. Intermediate magnifications documented crack-path tortuosity, step features, and secondary cracking. High magnifications examined local markings in the fatigue region and the morphology of dimples in the overload zone. Representative micrographs used in this work are labeled by position number (lower = nearer the crack-initiation site; higher = farther) and by magnification index—L (low), M (medium), H (high). EDS spot analyses were performed on matrix regions, dimple walls, and discrete particles identified at dimple bases.

3. Results

3.1. Spatially ordered fractography (near origin → far field)

Across the ordered series, the fracture surface separates into (i) a fatigue-propagation region near the origin, characterized by a comparatively smoother, step-rich topography with short secondary cracks, and (ii) a final fast-fracture (overload) zone in the far field, characterized by equiaxed microvoid dimples. Representative near-origin and mid-path fields (e.g., 10.0 L/M/H; 14.0 L/M/H; 15.5 L/M/H) show a predominantly transgranular fatigue surface with tortuous crack paths, step bands, and intermittent short secondary cracks (Fig. 1 and Fig. 2). Far-field panels (e.g., 18.0 L/M/H; 28.0 L/M/H) show a sharp morphological transition to a dimpled overload zone (Fig. 3).

3.2. Local markings in the fatigue region

In select high-magnification fields closer to the origin (e.g., 16.0H), localized parallel markings consistent with striations are visible; however, continuous periodic striations are not uniformly resolved across wider areas. The dominant appearance at low/medium magnification remains deflection-dominated (step bands, branching), as shown in medium-magnification panels (Fig. 1b).

3.3. Overload morphology and particle imprints

High-magnification far-field images (e.g., 16.5H; 27.5H; 28.0H) display uniform, equiaxed dimple arrays, indicative of ductile microvoid coalescence. Occasional particle imprints or residues at dimple bases are evident in several fields (Fig. 4b–c).

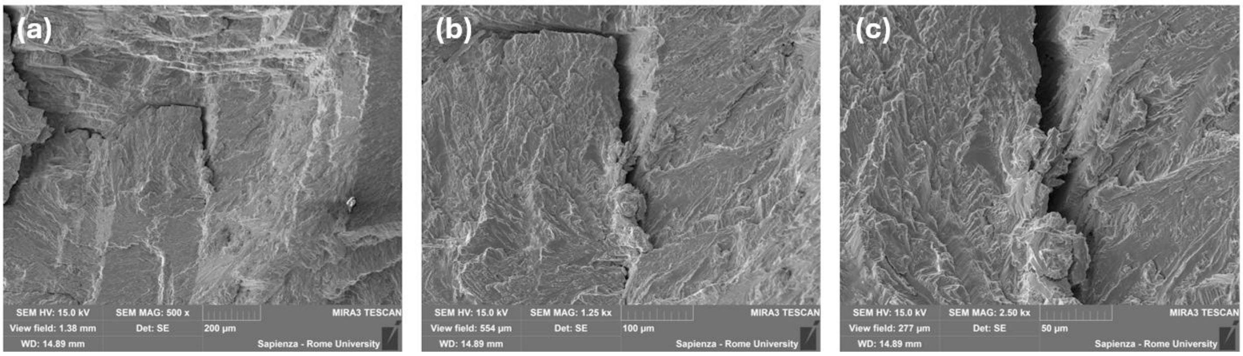

Fig. 1 Near-origin fracture surface (14.0 mm from the crack initiation). (a) Low magnification overview of the fatigue region; (b) medium magnification showing step bands and short secondary cracks (arrows); (c) high magnification of the fatigue surface. Fracture is predominantly transgranular; pervasive intergranular decohesion is not observed

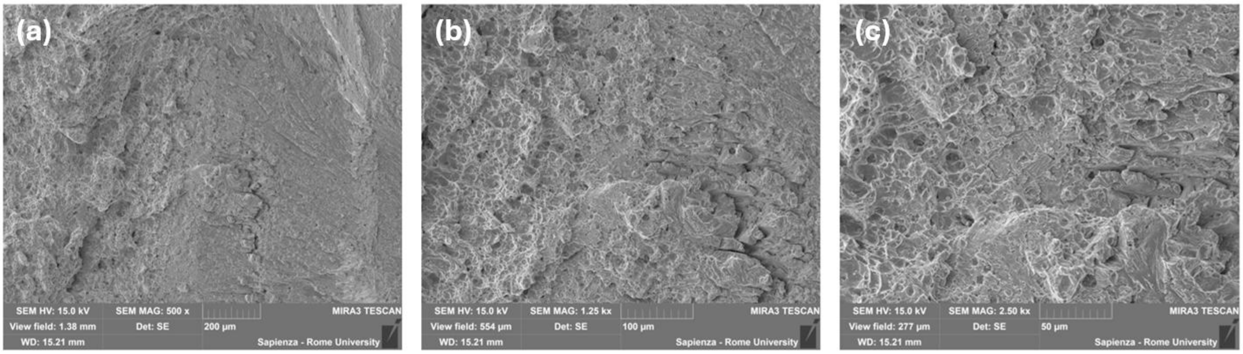

Fig. 2 Transition region (18.0 mm from the crack initiation). (a,b) Low/medium magnification illustrating the morphology change from fatigue propagation to final fracture; (c) high magnification showing emerging dimples.

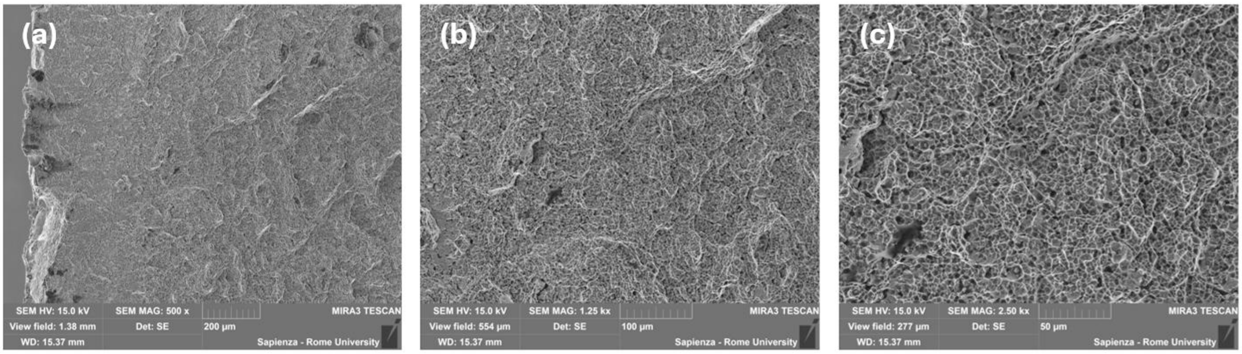

Fig. 3 Final overload zone (28.0 mm from the crack initiation). (a) Low magnification overview of the far-field surface; (b) medium magnification of the dimpled region; (c) high magnification showing equiaxed dimples indicative of ductile microvoid coalescence; an example particle imprint is indicated.

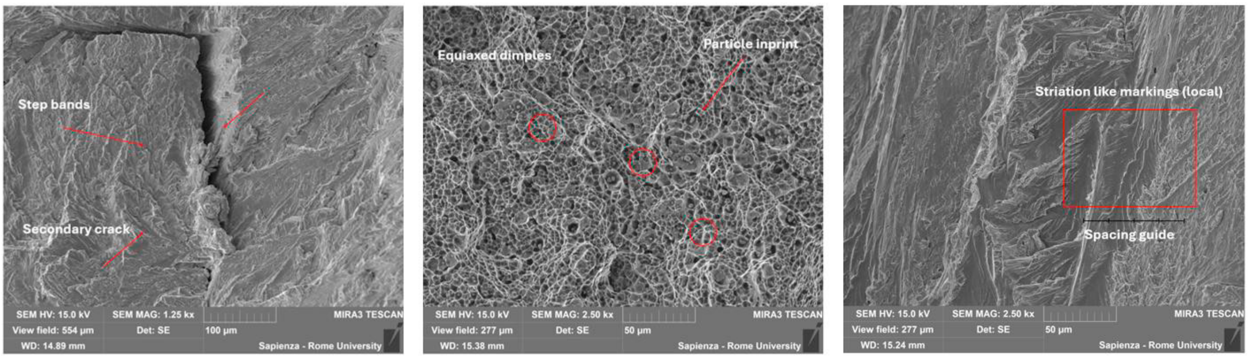

Fig. 4 (a) Medium magnification field with step bands and a secondary crack (arrows). (b) High magnification dimple field with circled dimples and a particle imprint. (c) High magnification near the origin showing localized striation-like markings (boxed) with a spacing guide.

3.4. EDS microanalysis

EDS spot checks on matrix regions within the fatigue area, on dimple walls in the overload zone, and on particles located at dimple bases detected the base elements Co, Cr, Fe, Mn, Ni at levels compatible with the nominal composition (Table 1). At particle sites, spectra show local compositional deviations relative to the matrix—frequently with oxygen—consistent with oxide/inclusion residues. No pervasive compositional banding was observed at the SEM/EDS length scale; chemical variations appear localized.

Table 1 EDS Analysis report

Element	Weight %	Atomic %	Net Int.	Error %	Kratio	Z	A	F
CrK	14.74	15.98	479.30	2.94	0.1671	1.0097	0.9920	1.1321
MnK	19.56	20.07	509.00	2.85	0.2094	0.9887	0.9942	1.0888
FeK	19.73	19.91	416.00	3.01	0.2045	1.0046	0.9803	1.0524
CoK	22.13	21.16	358.10	3.13	0.2131	0.9817	0.9693	1.0122
NiK	23.84	22.88	321.80	3.40	0.2339	1.0148	0.9628	1.0041

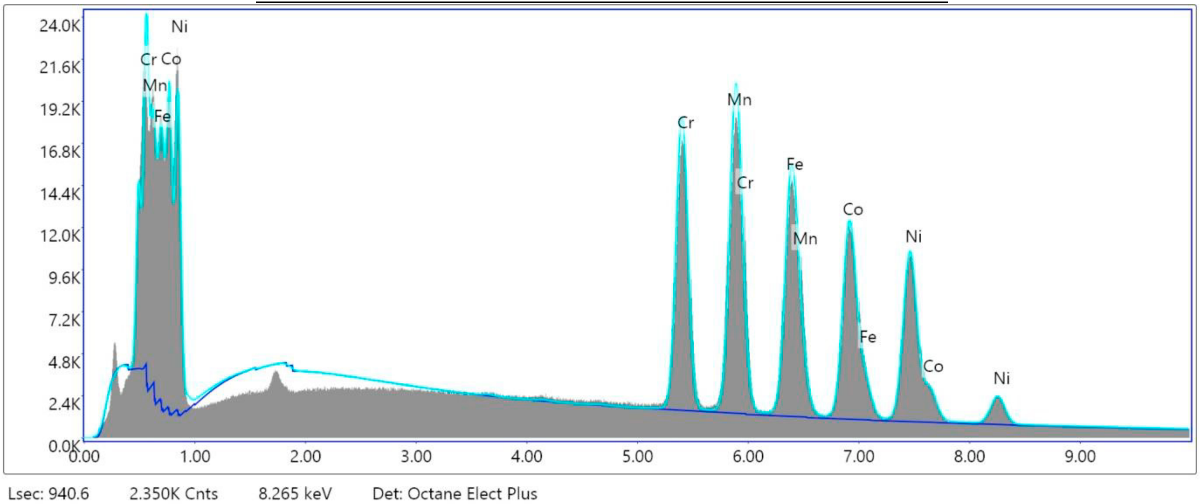

Fig. 5

4. Discussion

The spatial ordering reveals a systematic evolution of fracture morphology: a tortuous, transgranular fatigue surface with step bands and secondary cracking near the origin gives way to a dimpled overload texture approaching final failure. This progression is compatible with repeated crack-path deflection at microstructural barriers during fatigue, followed by microvoid nucleation and coalescence in the remaining ligament (Fig. 1–3).

Frequent step bands and secondary cracks indicate repeated deflection and branching of the crack front. Such topography is compatible with roughness-induced crack-closure contributions to the effective driving force (qualitatively); however, no closure quantification was attempted here. Striation-like markings appear locally in high-magnification fields near the origin, but their non-uniform visibility suggests that microstructural deflection is a prominent contributor at the examined length scales (Fig. 4a).

The equiaxed dimple morphology confirms ductile microvoid coalescence as the final fracture mechanism. Particle imprints at some dimple bases and local EDS deviations (including oxygen) support particle-assisted void nucleation. Outside these localized features, matrix chemistry appears uniform at the EDS scale, arguing against large-scale compositional banding as the primary driver of the fatigue-region morphology (Fig. 4b–c).

5. Conclusions

Fractographic evidence suggests that fatigue-crack growth in the equiatomic Co–Cr–Fe–Mn–Ni (Cantor) alloy is primarily transgranular. Close to the crack origin, locally ordered, striation-like markings suggest that the crack front advances due to cyclic slip. As the crack propagates, the presence of frequent step bands and occasional secondary cracks deflects the crack path and roughens the fracture surface. This is consistent with roughness-induced shielding, which reduces the effective driving force in the near-threshold regime. A clear morphological transition is then observed from the striated fatigue region to a dimpled overload zone, confirming ductile final fracture. The overload dimples are largely equiaxed and sporadic particle imprints or residues at their bases suggest microvoid nucleation at discrete inclusions, followed by coalescence. Notably, there is no pervasive intergranular decohesion and the crack path remains mostly transgranular, consistent with the alloy's stable FCC solid-solution character.

Taken together, these observations support a coupled mechanism in which intrinsic crack-tip plasticity (manifested as striations) operates alongside extrinsic shielding (arising from crack deflection and surface roughness) to control the evolution of crack growth from the near-threshold regime to the Paris regime. These results are consistent with previous reports on FCC high-entropy alloys and emphasise that microstructural homogeneity and stable slip promote damage tolerance, while controlled crack-path tortuosity can provide additional shielding. From an engineering standpoint, two practical approaches emerge for improving the resistance of FCC HEAs to fatigue-crack growth: introducing benign microstructural heterogeneity to encourage crack deflection without reducing ductility, and improving material cleanliness to limit microvoid nucleation at particles. Coupling future work that combines quantitative crack-growth kinetics with EBSD-resolved mapping of slip activity and crack-path crystallography would clarify how these factors determine the effective ΔK and further refine design strategies for damage-tolerant HEAs.

References

Bernd Gludovatz et al. ,A fracture-resistant high-entropy alloy for cryogenic applications.Science345,1153-1158(2014). https://doi.org/10.1126/science.1254581.

Gludovatz, B., Hohenwarter, A., Thurston, K. et al. Exceptional damage-tolerance of a medium-entropy alloy CrCoNi at cryogenic temperatures. Nat Commun 7, 10602 (2016). https://doi.org/10.1038/ncomms10602

Gludovatz, B., Ritchie, R.O. Fracture properties of high-entropy alloys. MRS Bulletin 47, 176–185 (2022). https://doi.org/10.1557/s43577-022-00267-9

Keli V.S. Thurston, Bernd Gludovatz, Anton Hohenwarter, Guillaume Laplanche, Easo P. George, Robert O. Ritchie, Effect of temperature on the fatigue-crack growth behavior of the high-entropy alloy CrMnFeCoNi, Intermetallics, Volume 88, 2017, Pages 65-72, ISSN 0966-9795, https://doi.org/10.1016/j.intermet.2017.05.009.

Keli V.S. Thurston, Bernd Gludovatz, Qin Yu, Guillaume Laplanche, Easo P. George, Robert O. Ritchie, Temperature and load-ratio dependent fatigue-crack growth in the CrMnFeCoNi high-entropy alloy, Journal of Alloys and Compounds, Volume 794, 2019, Pages 525-533, ISSN 0925-8388, https://doi.org/10.1016/j.jallcom.2019.04.234.

Tu-Ngoc Lam, Soo Yeol Lee, Nien-Ti Tsou, Hung-Sheng Chou, Bo-Hong Lai, Yao-Jen Chang, Rui Feng, Takuro Kawasaki, Stefanus Harjo, Peter K. Liaw, An-Chou Yeh, Ming-Jun Li, Ren-Fong Cai, Sheng-Chuan Lo, E-Wen Huang, Enhancement of fatigue resistance by overload-induced deformation twinning in a CoCrFeMnNi high-entropy alloy, Acta Materialia, Volume 201, 2020, Pages 412-424, ISSN 1359-6454, https://doi.org/10.1016/j.actamat.2020.10.016.

Tu-Ngoc Lam, Hsu-Huan Chin, Xiaodan Zhang, Rui Feng, Huamiao Wang, Ching-Yu Chiang, Soo Yeol Lee, Takuro Kawasaki, Stefanus Harjo, Peter K. Liaw, An-Chou Yeh, Tsai-Fu Chung, E-Wen Huang, Tensile overload-induced texture effects on the fatigue resistance of a CoCrFeMnNi high-entropy alloy, Acta Materialia, Volume 245, 2023, 118585, ISSN 1359-6454, https://doi.org/10.1016/j.actamat.2022.118585.

Linhu Shi, Zhe Zhang, Xu Chen, Fatigue crack growth behavior in CoCrFeMnNi high entropy alloy with harmonic structure topology, International Journal of Fatigue, Volume 172, 2023, 107656, ISSN 0142-1123, https://doi.org/10.1016/j.ijfatigue.2023.107656.

Simon Pillmeier, Michael Burtscher, Guillaume Laplanche, Reinhard Pippan, Jürgen Eckert, Anton Hohenwarter, On the fatigue crack growth behavior of nanocrystalline CrMnFeCoNi, International Journal of Fatigue, Volume 188, 2024, 108530, ISSN 0142-1123, https://doi.org/10.1016/j.ijfatigue.2024.108530.

Chen S, Fan X, Steingrimsson B, Xiong Q, Li W, Liaw PK. Fatigue dataset of high-entropy alloys. Sci Data. 2022 Jul 6;9(1):381. https://doi.org/10.1038/s41597-022-01368-5.

Brotzu, Andrea & Natali, Stefano & Zortea, Laura & Barbara, De. (2022). High Entropy Cantor Alloys (HEAs) modification induced by tungsten alligation, heat treatment and deep cold plastic deformation. Frattura ed Integrità Strutturale. 17. 309-320. https://doi.org/10.3221/IGF-ESIS.63.24.